

The Interdependence of Deformational and Thermal Processes in Mountain Belts

Audrey D. Huerta,* Leigh H. Royden, Kip V. Hodges

Crustal temperatures within collisional orogens are anomalously high compared with temperatures at comparable depths in stable continents, which is evidence of thermal processes that are fundamental to orogenesis. These temperatures can be explained by the redistribution of crust enriched in heat-producing elements through the accretion of crust from the down-going plate to the upper plate and surface erosion. With the use of geologically reasonable rates, the model results predict high temperatures (over 600°C) and inverted upper-plate geotherms (about 100°C over 20 kilometers) at shallow depths (20 to 40 kilometers) by 25 to 35 million years after collision. This study emphasizes the interdependence of deformational, surficial, and thermal processes.

Rocks present at the surface in many collisional orogens contain metamorphic mineral assemblages indicating high temperatures (~600° to 700°C) at midcrustal depths (20 to 30 km) (1). In some orogens this high-temperature metamorphism is associated with in situ partial melts (2), whereas less commonly, inverted metamorphic field gradients may develop within the upper plate (3, 4). Despite early suggestions that these phenomena could be explained by thrusting of hot rocks over cold rocks and by thickening of an upper crustal layer enriched in heat-producing elements (HPEs) during shortening (3, 5, 6), subsequent models that quantify the advection and conduction of heat during noninstantaneous thrusting have not reproduced observed thermal structures very well and are unable to explain steep-to-inverted metamorphic field gradients within the upper plate (7). Such shortcomings suggest that previous studies have neglected one or several processes that are responsible for the first-order thermal structure of collisional orogens.

Although previous studies have recognized the potential impact of HPE-enriched material within collisional belts (6, 8) and the importance of rapid surface denudation and accretion of material from the lower plate to the upper plate (9), our understanding of the thermal consequences of accretion and erosion on HPE-enriched crust has been limited to steady-state results (10). And although these results suggest that erosion and accretion can exert dramatic controls on the temperature structure, they are based on an idealized orogenic system in which the upper plate is HPE-enriched everywhere.

Here we present the results of a numer-

ical study addressing the time-dependent effects of erosion and accretion on the thermal structure of orogenic systems, using a more realistic distribution of HPE-enriched crust based on a simplified subduction zone geometry (Fig. 1). The contact between the upper and lower plates was assumed to have a uniform dip, at angle Θ . Convergence between upper and lower plates occurred at a constant rate v_c . Material was accreted from the lower to the upper plate at rate a , and material was removed from the surface of the upper plate at rate e (both measured in the vertical direction). The frame of reference was held fixed with respect to the toe of the upper-plate wedge, and material within the upper and lower plates moved with respect to the frame of reference. Standard finite difference techniques for calculation of conduction and advection of heat were used to compute the thermal evolution of the system. Initial thermal conditions were calculated as the steady-state conditions for subduction of a nonradioactive oceanic lithosphere at a convergence rate v_c , with no accretion across the subduction boundary or erosion at the surface. The upper plate initially contained an upper layer of HPE-enriched crust with heat production rate A and thickness d_r . Computation began at the time of collision ($t = 0$), as simulated by the introduction of lower plate continental crust with an HPE-enriched upper layer having heat production rate A and thickness d_r , and by the concomitant initiation of erosion and accretion. This was a highly idealized model of collision, inasmuch as it is not necessarily true that all three processes would begin simultaneously. We also ignored internal deformation within the upper and lower plates.

Accretion of HPE-enriched material from the lower plate to the upper plate resulted in the development of an HPE-enriched wedge (Fig. 2). The size and shape of this wedge were critical to the thermal evolution of the orogen. This triangular

wedge reached a maximum steady-state depth of

$$d_w = d_r \left(1 - \frac{e}{a} + \frac{v_c}{a} \sin \theta \right) \quad (1)$$

and a steady-state surface width of

$$s_w = \frac{d_w}{e/a \tan \theta} \quad (2)$$

at time

$$t_w = \left(\frac{d_r}{e} \right) \left(1 + \frac{v_c}{a} \sin \theta \right) \quad (3)$$

Initially, the upper plate was cold, with temperatures less than 300°C to depths in excess of 60 km. By $t = 8$ million years (My), temperatures within the toe of the upper plate had increased as HPE-enriched material was accreted to the upper plate and the HPE-enriched wedge began to form. By $t = 16$ My, temperatures within the upper plate increased to >400°C at a depth of 25 km. By $t = 24$ My, the thermal gradient had inverted, and a local temperature maximum in excess of 500°C had developed near the base of the HPE-enriched wedge in the upper plate at depths of 20 to 40 km. By $t = 32$ My, maximum temperatures within the upper plate were in excess of 600°C at depths of ~30 km, and maximum surface heat flow was on the order of 125 $\mu\text{W}/\text{m}^2$. From 32 My onward, temperatures changed relatively slowly within the evolving orogen and reached thermal steady state by about $t = 120$ My, at which

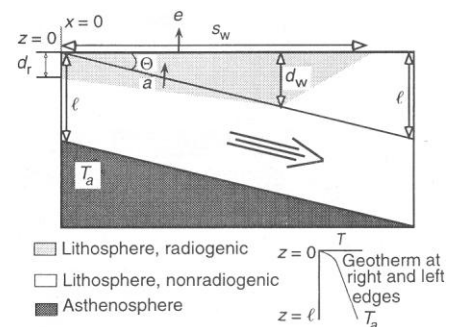


Fig. 1. Simplified subduction zone with dip Θ , convergence velocity v_c , and lithospheric thickness ℓ . Material is accreted from the lower to the upper plate at rate a (vertical component) and removed at the surface at rate e . The HPE-enriched wedge within the upper plate (light shaded area) has steady-state depth d_w and surface width s_w . Temperatures (T) are 0°C at $z = 0$ and T_a at the base of the lower plate. Dark shaded area indicates asthenosphere with $T = T_a$. Thermal boundary conditions at the right and left sides of the area modeled (at $x = 0$ and $x = \ell/\tan \theta$) for $z < \ell$ are steady-state temperatures for lithosphere with HPE-enriched crust to depth d_r , and are $d^2T/dx^2 = 0$ for $z > \ell$.

Department of Earth, Atmospheric, and Planetary Sciences, Massachusetts Institute of Technology, Cambridge, MA 02139, USA.

*To whom correspondence should be addressed.

time the temperature maximum ($>700^{\circ}\text{C}$) was located at a depth of about 30 km. The HPE-enriched wedge reached a steady-state shape by $t = 39$ My, with $d_w = 44$ km and $s_w = 225$ km.

Three parameters controlled steady-state maximum temperatures and inversion of geotherms: A , d_w , and v_c . The depth of the HPE-enriched wedge and the heat production rate had the most substantial impact on the thermal structure. Increasing either A or d_w (while all other parameters were held constant) resulted in substantially higher temperatures within the orogen and contributed to the inversion of geotherms within the upper plate; decreasing A or d_w

resulted in lower temperatures within the orogen and a lesser degree of inversion. Increasing the convergence velocity (holding all other parameters constant) resulted in slightly depressed temperatures at depths >15 km, especially near the subduction contact, and geotherms were more inverted; lower convergence velocities resulted in slightly higher temperatures and geotherms showed less inversion. Although the width of the wedge did not control the magnitude of maximum temperatures, increasing s_w (holding all other parameters constant) resulted in a broader region of elevated temperatures, with upper plate maximum temperatures located farther toward the hinter-

land. The transient thermal evolution was also primarily controlled by A , d_w , and v_c . High temperatures at shallow levels and inverted geotherms within the upper plate developed more quickly for higher values of v_c and d_w or for higher values of A , or both; high temperatures and inverted geotherms took longer to develop at lower values of v_c and d_w or lower values of A , or both.

There is a reasonably broad range of parameter values that yield inverted thermal gradients in the upper plate (for example, $A \geq 1.0$ for $d_w = 55$ km, or $A \geq 3.25$ for $d_w = 35$ km). However, in order to attain temperatures in excess of 600°C at depths as shallow as ~ 20 to 30 km as well as inverted geotherms in the upper plate, moderate values of A are required (for example, $A \geq 2.0$ for $d_w = 55$ km). In order to attain temperatures in excess of 600°C and inverted geotherms in a reasonable time span ($t < 40$ My), high values of A are required (for example, $A = 3.0$ for $d_w = 45$ km). Thus, we propose that the redistribution of HPE-enriched crust into a deep zone within the upper plate is an important factor in the thermal evolution of orogenic belts where high-temperature metamorphism, crustal melting, and geothermal inversions occur.

One of the best documented examples of high-temperature metamorphism associated with inverted metamorphic field gradients occurs in the central Himalayan orogen, where paleotemperatures increase structurally upward from a Miocene intracontinental subduction boundary (the Main Central thrust zone), reaching maximum temperatures in excess of 600°C at structural distances of 5 to 10 km above the Main Central thrust zone. Geologic data from some sectors of the orogen suggest that inverted field gradients in the Himalayas resulted from an actual inversion of the geothermal gradient (4, 11, 12); in other areas, the observed field gradients have been interpreted as the result of late- or post-metamorphic structural disruption (13). Although the structural inversion of field gradients requires no special thermal circumstances, the documentation of high-grade metamorphism and inverted geothermal gradients in the Himalayas has inspired many researchers to propose that transient heat sources such as dissipative heating, mantle delamination, or other mechanisms (14) are responsible for the observed metamorphic conditions.

Comparison of the nature and timing of Himalayan metamorphism and the results presented here suggests that the effects of accretion and erosion and the attendant redistribution of HPE-enriched crust offer an alternative explanation for the development of high temperatures and inverted

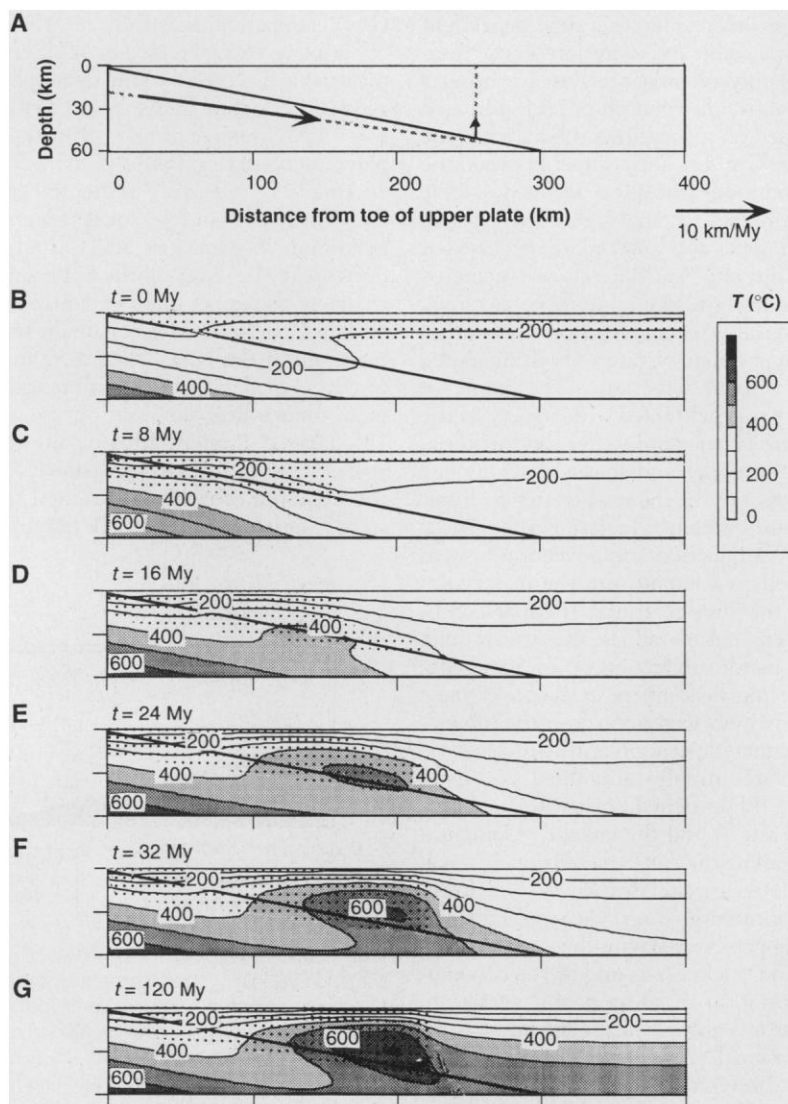


Fig. 2. Crustal cross sections for the model outlined in Fig. 1, based on $\tan \Theta = 0.2$, $v_c = 20$ km/My, $a = 1.6$ km/My, $e = 1.6$ km/My, and $\ell = 126$ km. (A) Material velocity fields. (B through G) Thermal evolution and growth of HPE-enriched wedge, from $t = 0$ My (initiation of collision) to $t = 120$ My (approximately steady state). Stippled pattern indicates HPE-enriched crust with $A = 3 \mu\text{W}/\text{m}^3$. Other parameters were as follows: $d_f = 18$ km and $T_a = 1260^{\circ}\text{C}$. The width of the area modeled was 630 km, thermal conductivity was 2.5 W/mK, and thermal diffusivity was 10^{-6} m²/s. Note the inversion of geothermal gradients and a local temperature maximum in excess of 600°C at depths <30 km within the upper plate by $t = 32$ My.

geothermal gradients within collisional orogens. Within the central Himalayas, the development of inverted field gradients, accompanied by substantial crustal melting, occurred at about 20 to 25 million years ago, about 25 to 35 My after the initiation of collision between India and Eurasia (15). Rocks currently at the surface were at depths of 20 to 40 km during regional metamorphism (12, 16), yielding averaged rates of denudation of 1 to 2 km/My. Likewise, extensive tracts of lower (Indian) plate rocks with an exposed surface width greater than 300 km have been accreted episodically onto the upper (Eurasian) plate since the time of collision. Paleosubduction rates are unconstrained, but modern rates of convergence across the Himalayas are about 10 to 25 km/My (17). Radioactive heat production rates for metamorphic and igneous rocks of the Himalayas range from ~ 1.5 to $>6 \mu\text{W}/\text{m}^3$, with a significant proportion ($>25\%$) of reported values in excess of $4 \mu\text{W}/\text{m}^3$ (18). Thus, parameter values (especially $A = 3 \mu\text{W}/\text{m}^3$) used to construct Fig. 2 are consistent with observations from the Himalayas. The agreement between timing, paleotemperatures and depths recorded in the central Himalayas, and the modeled thermal structure 32 My after collision (Fig. 2) suggests that redistribution of material with a high rate of heat production within the Himalayan orogen may have been an important factor in its thermal evolution.

Our model suggests that accretion and erosion and the attendant redistribution of HPE-enriched material exert first-order control on the thermal and metamorphic evolution of collisional orogens. Accretion leads to the development and maintenance of a wedge of HPE-enriched material within the upper plate of intracontinental subduction zones. Surface erosion also controls the geometry of this wedge and enhances heating within the upper plate by advecting material from deeper to shallower crustal levels.

REFERENCES AND NOTES

1. R. D. Hatcher Jr. et al., in *The Appalachian-Ouachita Orogen in the United States*, R. D. Hatcher Jr., W. A. Thomas, G. W. Viele, Eds. (Geological Society of America, Boulder, CO, 1989), pp. 233–318; A. Ganser, *Geology of the Himalayas* (Wiley Interscience, London, 1964).
2. W. S. Pitcher, *Geol. Rundsch.* **76**, 51 (1987).
3. P. Le Fort, *Am. J. Sci.* **275A**, 1 (1975).
4. M. S. Hubbard, *J. Metamorph. Geol.* **7**, 19 (1989).
5. E. R. Oxburgh and D. L. Turcotte, *Schweiz. Mineral. Petrogr. Mitt.* **54**, 641 (1974).
6. P. C. England and A. Thompson, in *Collision Tectonics*, M. P. Coward and A. C. Ries, Eds. (Special Publication 19, Geological Society of America, Boulder, CO, 1986), pp. 83–94.
7. P. Bird, M. N. Toksoz, N. H. Sleep, *J. Geophys. Res.* **80**, 4405 (1975); Y. Shi and C. Y. Wang, *Geology* **15**, 1048 (1987); P. Karabinos and R. Ketchum, *J. Metamorph. Geol.* **6**, 559 (1988); C. Ruppel and K. V. Hodges, *Tectonics* **13**, 17 (1994).

8. C. Pinet and C. Jaupart, *Earth Planet. Sci. Lett.* **84**, 87 (1987).
9. F. A. Dahlen and T. D. Barr, *J. Geophys. Res.* **94**, 3906 (1989); T. D. Barr and F. A. Dahlen, *ibid.*, p. 3923; S. M. Peacock, in *Metamorphism and Crustal Evolution, Western Conterminous United States*, W. G. Ernst, Ed. (Prentice-Hall, Englewood Cliffs, NJ, 1987), pp. 953–975.
10. L. H. Royden, *J. Geophys. Res.* **98**, 4487 (1993).
11. K. V. Hodges, P. Le Fort, A. Pêcher, *Geology* **16**, 707 (1988).
12. A. Pêcher, *J. Metamorph. Geol.* **7**, 31 (1989).
13. M. Brunel and J. R. Kienast, *Can. J. Earth Sci.* **23**, 1117 (1986); M. P. Searle and A. J. Rex, *J. Metamorph. Geol.* **7**, 127 (1989).
14. P. Molnar and P. England, *J. Geophys. Res.* **95**, 4833 (1990); G. A. Houseman, D. P. McKenzie, P. Molnar, *ibid.* **86**, 6115 (1981).
15. M. S. Hubbard and T. M. Harrison, *Tectonics* **8**, 865

- (1989); K. V. Hodges et al., *Contrib. Mineral. Petrol.* **117**, 151 (1994); M. P. Searle, D. J. W. Cooper, A. J. Rex, in *Tectonic Evolution of the Himalayas and Tibet*, R. M. Shackleton, J. F. Dewey, B. F. Windley, Eds. (The Royal Society, London, 1988), pp. 117–150.
16. K. V. Hodges, M. S. Hubbard, D. S. Silverberg, *Philos. Trans. R. Soc. London Ser. A* **326**, 257 (1988).
17. H. Lyon-Caen and P. Molnar, *Tectonics* **4**, 513 (1985).
18. B. C. Scaillet, C. France-Lanord, P. Le Fort, *J. Volcanol. Geotherm. Res.* **44**, 163 (1990); P. Vidal, A. Cocherie, P. Le Fort, *Geochim. Cosmochim. Acta*, **46**, 2279 (1982); A. M. Macfarlane, thesis, Massachusetts Institute of Technology (1992).
19. We thank two anonymous reviewers for helpful comments. Support was provided by NSF grant EAR 9418062 to K.V.H.

1 April 1996; accepted 12 June 1996

Lithologic Control of the Depth of Earthquakes in Southern California

Harold Magistrale* and Hua-wei Zhou

The depth distribution of southern California earthquakes indicates that areas underlain by schist basement rocks have a shallower (4 to 10 kilometers) maximum depth of earthquakes than do areas with other types of basement rocks. The predominant minerals in the schists become plastic at lower temperatures, and thus at shallower depths, than the minerals in the other basement rocks. The lateral variations in lithology will control the depth extent (and thus the magnitudes) of potential future earthquakes; these depths can be determined from the depth of the current background seismicity.

Earthquake magnitude is proportional to fault area. The fault area is the product of the length and the width of the fault on which brittle rupture occurs. Attempts to determine the magnitude of potential future earthquakes must therefore consider factors that influence the depth extent of rupture. Here we examine variations in the maximum depth of earthquakes in southern California and correlate a relatively shallow maximum depth to the presence of schist basement rocks.

The Late Cretaceous–early Tertiary Pelona, Orocopia, and Rand schists are structurally low rocks exposed in sparse outcrops (1) (Fig. 1). The schists are in low-angle fault contact with the overlying crystalline rocks (1–5). The emplacement mechanism of the mostly graywacke protolith is controversial: It is either in a west-dipping subduction zone under a continental fragment that was then accreted to western North America (3, 4) or in an east-dipping subduction zone under the western North American margin (5–7). Subsequent faulting and uplift have exposed the schists. Seismic reflection surveys show that the

schists extend over a large lateral area in the subsurface (8–11) and are >7 km thick (12). These surveys and the regional distribution of the schists (1, 3–7) indicate that they probably underlay much of onshore southern California. Similarly, much of the inner continental borderland offshore of southern California is underlain by the Mesozoic Catalina Schist (13–15). This schist also has only sparse surface outcrop, but seismic reflection surveys and borehole samples indicate a widespread subsurface extent (14, 15).

Recently, Zhou inverted southern California earthquake arrival times for crustal velocities and hypocenters (16). About 37,000 well-recorded earthquakes detected on the southern California seismic network (SCSN) between 1981 and 1994 provided data for the inversion (17). These earthquakes are representative of the more extensive SCSN earthquake catalog. We use the new hypocenters (Fig. 2) to examine variations in the hypocenter depths.

A major feature in the hypocenter depths is a 4- to 10-km change, or step, in the maximum depth of hypocenters. The step is particularly evident in the San Geronio Pass area (Fig. 2) as a result of the high density of hypocenters (18, 19). The step can be traced as a regional feature that follows the San Andreas fault in the Coach-

H. Magistrale, Department of Geological Sciences, San Diego State University, San Diego, CA 92182, USA.
H.-w. Zhou, Department of Geosciences, University of Houston, Houston, TX 77204, USA.

*To whom correspondence should be addressed.